International Journal of GEOMATE, Dec., 2025 Vol.29, Issue 136, pp.121-130
ISSN: 2186-2982 (P), 2186-2990 (O), Japan, DOI: https://doi.org/10.21660/2025.136.g15120
Geotechnique, Construction Materials and Environment

A NEW OPERATION PRINCIPLE OF SYSTEM THAT COMBINES PHASE-CONTROLLED ACTUATOR WITH DIFFERENT DRIVE FREQUENCIES

Hiroyuki Yaguchi[1] and Sota Abe[1]

[1] Faculty of Engineering, Tohoku Gakuin University, Japan

*Corresponding Author, Received: 18 April 2025, Revised: 04 Nov. 2025, Accepted: 06 Nov. 2025

ABSTRACT: In Japan, the shortage of construction workers and inspectors has become a social problem due to the declining birthrate and aging population. In addition, the slow progress of automation in challenging environments, such as construction sites and bridges, has been pointed out. Although various types of inspection robot have been developed, bridge inspection technology has not been fully established. In this study, the operation of a phase-controlled actuator equipped with vibration components with different drive frequencies is investigated. The phase-controlled actuator, in which a second-harmonic vibration component is coupled to a fundamental-wave vibration component to avoid vibration interference, exhibits excellent propulsive characteristics. To further improve the propulsion characteristics, a prototype actuator system, in which two phase-controlled actuators with different drive frequencies are coupled, is developed. Tests on prototypes show that this system can simultaneously achieve high-speed movement and good traction characteristics. Furthermore, the operation principle of this actuator system is established based on test results. The potential of an inspection device with the proposed actuator for the internal inspection of bridges with a small automatic tapping device is demonstrated.

Keywords: Actuator system, Operation principle, Second-harmonic vibration, Phase control, Inspection

1. INTRODUCTION

In Japan, the shortage of construction workers and inspectors has become a social problem due to the declining birthrate and aging population. The number of workers in the construction industry has decreased from 6.85 million in 1997 to 4.77 million in 2024. Furthermore, starting in 2025, the number of workers is expected to decrease by more than 100,000 per year. In the general manufacturing industry, task automation is relatively easy using industrial robots and artificial intelligence. However, automation in challenging environments, such as construction sites and bridges, is lagging behind. In particular, bridge inspection requires the operator to approach and touch the part to be inspected. Currently, inspection vehicles, aerial lifts, and boats are used to approach bridges, making bridge inspection dangerous and difficult. Since 2023, the 730,000 road bridges in Japan have to be inspected every 5 years. Various inspection robots have thus been developed to ensure worker safety and improve work efficiency.

Several inspection robots based on mechanisms that allow movement on walls, such as magnetic wheel systems [1, 2], electromagnet systems [3], suction systems with negative pressure [4], crawler-type systems [5, 6], and coupled vibration and suction systems [7], have been proposed. These inspection robots use a number of electromagnetic motors as the drive source, giving them good controllability. However, even robots equipped with large electromagnetic motors that have good torque characteristics exhibit significant degradation of movement characteristics when moving in a vertical plane. On the other hand, small electromagnetic motors lack torque, making it difficult to move on vertical surfaces. There is thus a limit to the improvement in robot movement characteristics that can be achieved by changing electromagnetic motors.

In recent years, drone-type flying robots have been developed [8, 9]. Although drones can perform inspection work in hazardous areas, they cannot perform inspections using automatic tapping devices**.** Furthermore, drone flights are affected by weather conditions and inspection technology for bridges using drones has not yet been established.

Generally, vibration and noise are considered harmful in engineering, and vibration control is applied [10-12]. On the other hand, as an example of vibration utilization, the authors previously proposed a phase-controlled actuator capable of movement on magnetic materials [13, 14]. In addition, the present authors previously proposed an actuator for structural testing that consists of eight identical vibration components arranged in a square acrylic frame [15]. A prototype of this actuator was shown to be capable of rotational and translational reciprocating motion. However, vibration interference between the vibration components degraded the movement characteristics.

In this study, a phase-controlled actuator with vibration components with different drive frequencies is proposed. The phase-controlled actuator, in which a second-harmonic vibration component is coupled to a fundamental-wave vibration component to avoid vibration interference, exhibits excellent propulsive characteristics. To further improve the propulsive characteristics, an actuator system in which two phase-controlled actuators with different drive frequencies are coupled is proposed. The operation principle of this actuator system is studied and its driving principle is established based on the results of tests on prototypes.

Measurements show that this actuator system can simultaneously achieve high-speed movement and good traction characteristics, which are usually in conflict with each other. This paper demonstrates the potential of an inspection device with the proposed actuator that can realize internal inspections of bridges with a compact automatic tapping device.

2. RESEARCH SIGNIFICANCE

The inspection of bridges and other structures has become an important issue in Japan due to the aging of infrastructure. However, the inspection of bridges over waterways (e.g., rivers, seas, and lakes) is extremely difficult. Although many inspection robots have been developed for visual or internal inspection, inspection techniques have not yet been established.

Devices for driving robots are almost exclusively limited to electromagnetic motors due to their high controllability. When electromagnetic motors are used as robot actuators, additional components such as reduction gears become necessary, increasing the robot's weight. Therefore, the development of actuators capable of direct drive is essential. The authors proposed a vibration actuator capable of direct drive. However, equipping it with multiple vibration components to improve movement characteristics led to a problem where vibration interference caused a deterioration in movement performance. The first significance of this research is the invention of a new method to eliminate vibration interference between the vibration components, confirmed through actual machine testing. Building on this, the second significance of this research is establishing a new operating principle that substantially improves the propulsion characteristics of the vibration actuator previously proposed by the authors. Thus, by combining vibration components with different drive frequencies, we have developed a device that simultaneously achieves high-speed movement and high propulsion characteristics, capabilities previously unattainable with electromagnetic motors. Furthermore, the third significance of this research is the realization of an actuator system capable of reciprocating linear and rotational movement without vibration interference. By realizing robots driven by these actuator systems, future applications could enable internal inspections of large steel structures.

3. PHASE-CONTROLLED ACTUATOR

3.1 Structure of Phase-controlled Actuator

Figs. 1(a) and 1(b) show the two types of phase-controlled actuator prototyped in this study, I and II, with multiple vibration components with the same specifications mounted in an acrylic frame (thickness: 5 mm, width: 15 mm, length 50 mm). Actuator I has vibration components A and B in an orthogonal arrangement. Actuator II has vibration components B and C coaxially arranged and vibration component A orthogonally aligned with components B and C. The stainless steel coil spring that constitutes a vibration component has an outer diameter of 12 mm, a free length of 32 mm, and a spring constant of 2,016 N/m. The NdFeB permanent magnet (diameter: 12 mm, height: 6 mm) at the top of each coil spring is magnetized in the height direction. The electromagnet consists of a 4.2-mm-diameter iron core with a 0.18-mm-diameter copper wire wound 1080 turns. The gap between the iron core and the permanent magnet in the static state is 5 mm. As shown in Fig. 1, height-magnetized NdFeB magnets (diameter: 10 mm, height: 2 mm) were mounted at the center of the acrylic frame and on each side 20 mm from the center. A 1-mm-thick rubber sheet was glued onto each of these magnets to increase the frictional force. The permanent magnets mounted on the sides of the center section stabilize the linear movement of the actuator. The positions of the permanent magnets were determined based on preliminary experiments. Actuator I is 53 mm high, 83 mm long, and 15 mm wide and has a total mass of 45.1 g. Actuator II is 53 mm high, 116 mm long, and 15 mm wide and has a total mass of 63.5 g.

3.2 Operation Principle of Phase-controlled Actuator

To illustrate the operation principle of the phase-controlled actuator, the displacement coordinates x and y are defined as shown in Fig. 1(b). The operation principle applies to both phase-controlled actuators I and II. The operation of actuator II is described here. Vibration components B and C are assumed to vibrate in phase in the x-direction. As shown in Fig. 2, when the actuator is set on a magnetic material, the attractive force of each of the three permanent magnets is P. The total attractive force $3P$ holds the actuator and allows the vibration

components to vibrate.

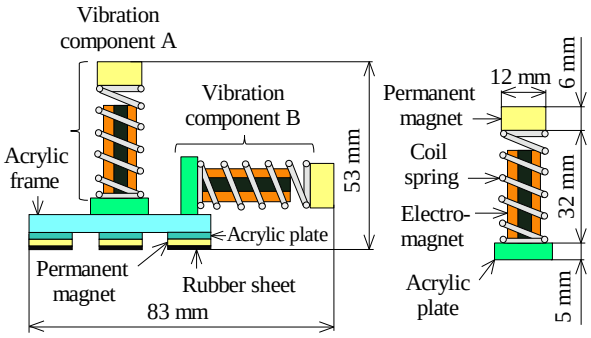

(a) Actuator I and vibration component

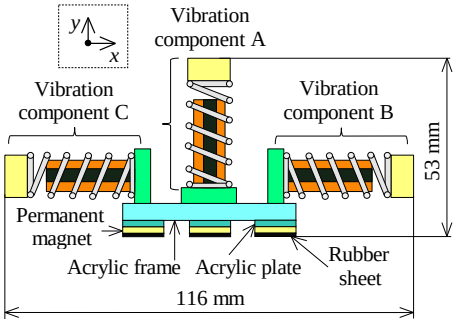

(b) Actuator II

Fig. 1 Structure of phase-controlled actuator

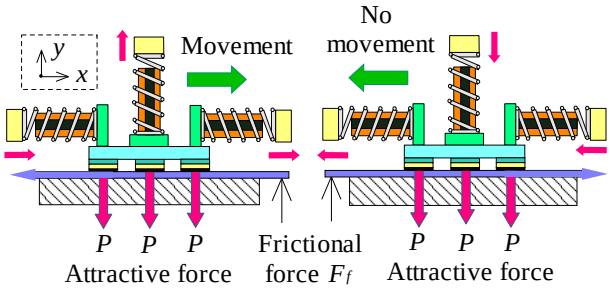

(a) Movement (b) No movement

Fig. 2 Principle of locomotion for proposed actuator

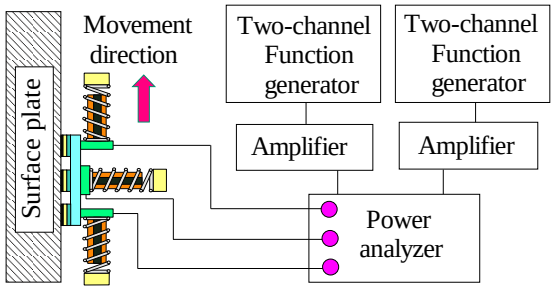

Fig. 3 Experimental apparatus

As shown in Fig. 2(a), when vibration component A is displaced in the $+y$ direction, friction force F_f decreases due to the force generated by the permanent magnet. In this state, when components B and C are displaced in the $+x$ direction, the actuator moves in the $+x$ direction due to the force generated by the permanent magnets. On the other hand, as shown in Fig. 2(b), when the permanent magnet of vibration component A is displaced in the $-y$ direction, friction force F_f increases and the actuator does not move when components B and C are displaced in the $-x$ direction. Therefore, the actuator can move only in the $+x$ direction.

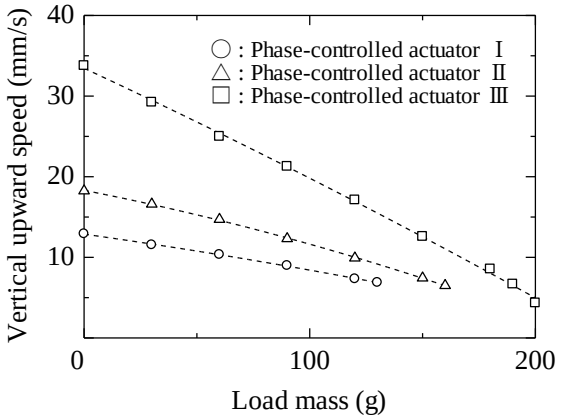

Fig. 4 Relationship between load mass and vertical upward speed

Table 1 Vibration amplitude of each vibration component

Driving component (250 mA)	Amplitude of vibration component (mm)		
	A	B	C
A	3.90	0	0
B	0	3.26	2.36

3.3 Movement Characteristics of Phase-controlled Actuator

Fig. 3 shows a schematic diagram of the experimental setup. An iron surface plate (width: 300 mm, length: 300 mm, thickness: 60 mm) was used as the magnetic material. Two 2-channel signal generators with variable phase capability and two power amplifiers were used to resonantly drive the vibration components mounted on the phase-controlled actuator. The resonant frequency of each vibration component was 90.5 Hz. The AC current input to the electromagnets inserted in the vibration components was measured using a power analyzer. Hereafter, the AC current input to the electromagnet is reported as an effective value. The attractive force on the permanent magnet to which the rubber sheet is attached is P = 2 N. Thus, the total pull force of the actuator is 6 N.

Phase-controlled actuators I and II were set on a vertical plane. Fig. 4 shows the relationship between the load mass attached to the actuators and the

vertical upward speed, with the input current to vibration component A set at 60 mA and that to vibration component B (= C) set at 250 mA. The load mass was attached to the acrylic frame of the actuator using string. From this figure, the propulsion characteristics of actuator II are only about 1.45 times, not twice, those of actuator I. The reason for this is likely vibration interference between the vibration components, which have the same dimensions.

Table 1 shows the vibration amplitudes of vibration components A, B, and C for phase-controlled actuator II when the electromagnet was driven resonantly with an input current of 250 mA. The vibration amplitudes were measured using a laser displacement meter and a digital oscilloscope. When vibration component A is driven, components B and C are orthogonally aligned, so there is no vibration interference between the vibration components.

On the other hand, when vibration component B is driven, the vibration wave propagates to component C. Since vibration components B and C vibrate symmetrically around the center of the frame, the interference between them is very large. Antisymmetric vibration of vibration components B and C is necessary for the actuator to move. This requires that a large input current be applied to vibration component C. The addition of a vibration component with the same characteristics is not a viable solution for improving the propulsive characteristics due to the vibration interference problem.

4. COUPLING OF VIBRATION COMPONENTS WITH DIFFERENT DRIVE FREQUENCIES

From the point of view of vibration, to completely prevent vibration interference between vibration components, the vibration frequency of one of the two components must be at least twice that of the other component. To eliminate vibration interference, vibration components with different frequencies (denoted as actuator III) were installed and investigated.

Fig. 5 shows the displacements (x and y) of vibration components A, B, and C versus ωt, where ω is the angular frequency and t is time. In the figure, the second, third, and fourth harmonics are shown with respect to the fundamental wave ω, with the initial phase varying as in Eq. (1).

$$\left.\begin{aligned} y &= \sin \omega t \\ y &= \sin 2\omega t - \pi/2 \\ y &= \sin 3\omega t - \pi \\ y &= \sin 4\omega t + \pi \end{aligned}\right\} \quad (1)$$

The solid and dashed black lines in the figure

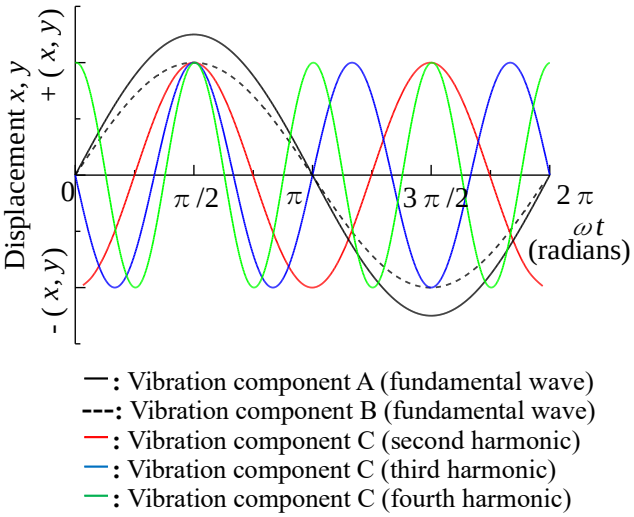

Fig. 5 Fundamental wave and second, third, and fourth harmonics

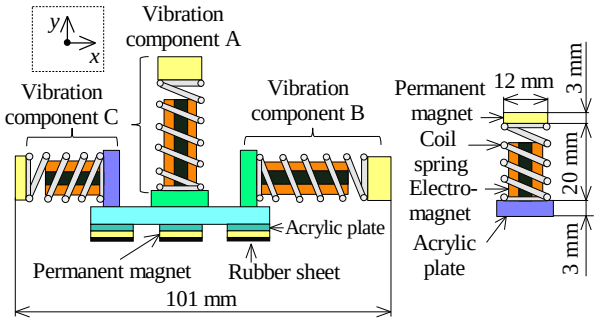

(a) Component C with different drive frequencies (b) Component with second harmonic

Fig. 6 Phase-controlled actuator III

show the vibration displacements of vibration components A and B, respectively, shown in Fig. 6(a) for the fundamental wave. The red, blue, and green lines show the vibration displacements of vibration component C shown in Fig. 6(a) for the second, third, and fourth harmonics, respectively, of vibration components A and B. As shown in Fig. 2, in the operation principle of the phase-controlled actuator, displacements x and y of fundamental-wave vibration components A and B are synchronized with a phase difference of 0 degrees.

The relationship between the second harmonic (red line) and fundamental-wave vibration component A (black line) is next discussed, including the displacement coordinates x and y in Fig. 6(a). As shown earlier, friction force F_f decreases (increases) when vibration component A is displaced in the $+x$ ($-x$) direction.

In Fig. 5, at ωt = 0 or π, the actuator does not move in the $-x$ direction when second-harmonic vibration component C is displaced in the $-x$ direction, because vibration component A is in a

neutral state. On the other hand, at $\omega t = \pi/2$, friction force F_f decreases as vibration component A is displaced in the $+y$ direction. In this condition, when second-harmonic vibration component C is displaced in the $+x$ direction, the actuator tends to move in the $+x$ direction. In the range $\omega t > \pi$, friction force F_f increases as vibration component A is displaced in the $-y$ direction and the actuator does not move when vibration component C is displaced in the $+x$ direction. Therefore, the combination of the fundamental wave and the second harmonic allows the actuator to move in the intended direction (i.e., the $+x$ direction).

Consider the third harmonic (blue line) and the fundamental wave (black line) in Fig. 5. For $0 < \omega t < \pi$, fundamental-wave vibration component A is displaced in the $+y$ direction and friction force F_f decreases. In this range, third-harmonic vibration component C makes one half-period motion in the $+x$ direction and two half-period motions in the $-x$ direction, so the actuator is expected to move less in the $+x$ direction. Furthermore, in the range $\omega t > \pi$, frictional force F_f increases due to the vibrational displacement of vibration component A. Thus, even if vibration component C is displaced in the $+x$ direction, the actuator cannot move in the intended direction (i.e., the $+x$ direction).

If the direction of movement of the actuator can be controlled by a combination of the fundamental wave and the second harmonic, the fourth harmonic, whose frequency is twice that of the second harmonic, can be considered an applicable frequency.

The measurement results show that the movement characteristics of actuator III are more than twice those of actuator II. The combination of the fundamental wave and the second harmonic, which does not cause vibration interference between the vibration components, is a very effective method for improving the propulsive characteristics of the actuator.

5. ACTUATOR SYSTEM WITH TWO COUPLED PHASE-CONTROLLED ACTUATORS

5.1 Structure and Operation Principle

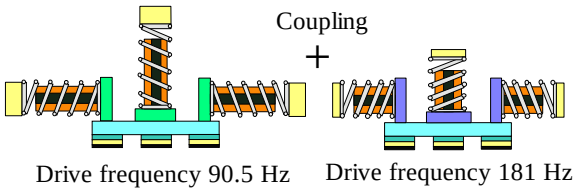

(a) Fundamental wave (b) Second harmonic

Fig. 7 Coupling of two phase-controlled actuators

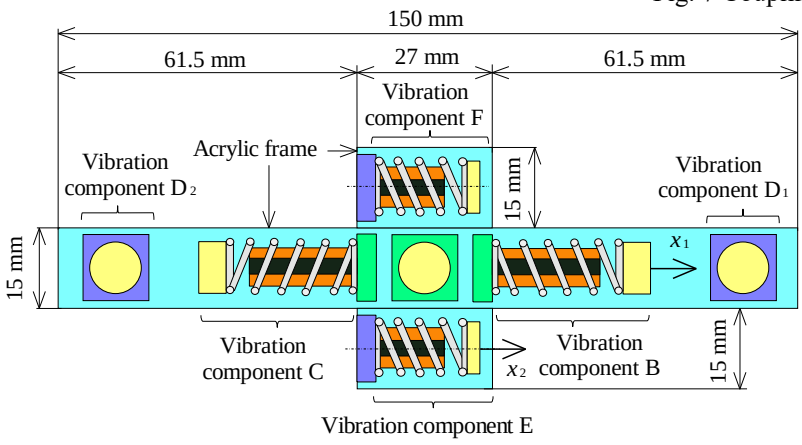

(a) Plan view

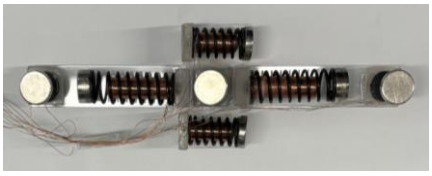

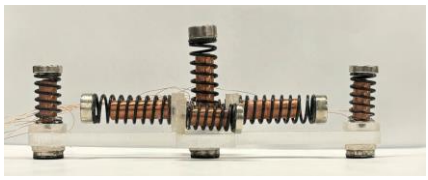

(c) Photographs

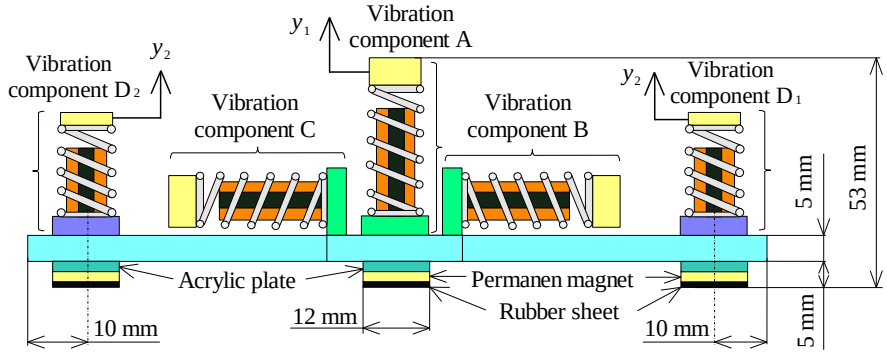

(b) Front view (excluding vibration component E and F)

NdFeB permanent magnet (diameter: 12 mm, height: 3 mm) is magnetized in the height direction. The

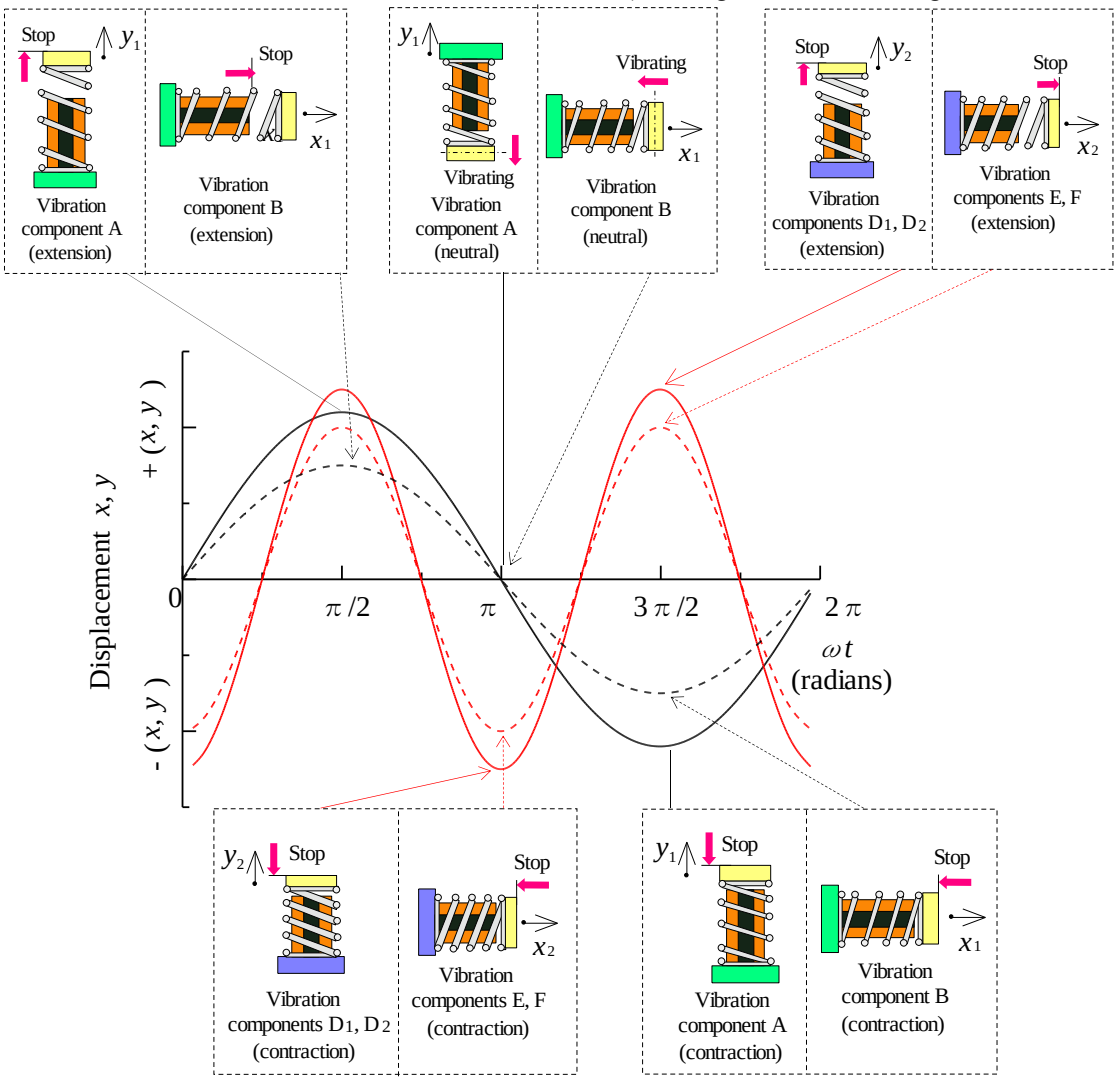

—: Vibration component A (fundamental wave)
—: Vibration components D_1, D_2 (second harmonic)
---: Vibration component B (fundamental wave)
---: Vibration components E, F (second harmonic)

Fig. 9 Operation principle of actuator system (displacement and generated force of each vibration component)

To further improve the propulsion characteristics, a prototype actuator system was developed in which phase-controlled actuators with fundamental-wave and second-harmonic vibration components are coupled, as shown in Fig. 7. The drive frequencies for the fundamental-wave and second-harmonic vibration components are 90.5 and 181 Hz, respectively.

As shown in Fig. 6(a), a prototype of phase-controlled actuator III with vibration component C (see Fig. 6(a)), whose frequency is the second harmonic with respect to the fundamental wave, was developed. As shown in Fig. 6(b), the stainless steel coil spring that constitutes vibration component C has an outer diameter of 11 mm, a free length of 20 mm, and a spring constant of 3,926 N/m. The electromagnet consists of a 3.2-mm-diameter iron core around which 0.18-mm-diameter copper wire was wound 880 turns. The gap between the iron core and the permanent magnet is 3 mm. The resonant frequency of second-harmonic vibration component C is 181 Hz. Except for vibration component C, the vibration components are identical to the actuator shown in Fig. 1(b). Preliminary experiments confirmed that no vibration interference occurs between the electromagnets of vibration components A, B, and C when they are each driven resonantly by applying a current of 250 mA. As shown in Fig. 5, the initial phases in the fundamental-wave and second-harmonic vibration components were adjusted using the 2-channel signal generator.

The movement speed of actuator III was measured

when the same input current as that for the fundamental-wave vibration component was applied to second-harmonic vibration component C. The obtained results are shown in Fig. 4 (square coupled, as shown in Fig. 7. The drive frequencies for the fundamental-wave and second-harmonic vibration components are 90.5 and 181 Hz, respectively.

Fig. 8 shows the prototype actuator system. In this actuator system, three fundamental-wave vibration components (A, B, and C) are mounted within an acrylic frame (thickness: 5 mm, length: 150 mm). The combination of these components is denoted as type I. In addition, four second-harmonic vibration components (D_1, D_2, E, and F) are mounted. This combination is denoted as type II. This actuator system has second-harmonic vibration components E and F attached in parallel to enable rotational motion in addition to linear reciprocating motion. The fundamental-wave and second-harmonic vibration components were tuned to have the same vibration characteristics. For each vibration component, the displacement coordinates x_1, x_2 and y_1, y_2 were defined as shown in Fig. 8. When the actuator system moves, vibration components B and C vibrate anti-symmetrically with respect to displacement coordinate x_1. Vibration components E and F are displaced in the same direction with respect to displacement coordinate x_2.

The three permanent magnets and the rubber sheets attached to the bottom of the actuator system have the same dimensions as those for the actuators shown in Fig. 1. This actuator system is 53 mm high, components A and B (C is antisymmetric with B). 150 mm long, and 45 mm wide and has a total mass of 120 g.

Next, the operation principle of the combined type I and type II phase-controlled actuators is considered. Fig. 9 shows the displacements (x_1, x_2 and y_1, y_2) of the fundamental-wave and second harmonic vibration components with the initial phase adjusted versus ωt. The black solid and dashed lines show the vibration displacements of fundamental-wave**.** The red solid and dashed lines show the vibration displacements of second-harmonic vibration components D_1, D_2 and E, F, respectively.

In Fig. 9, at ωt = 0 or π, fundamental-wave vibration components A and B (C vibrates anti-symmetrically with B) are neutral. On the other hand, since second-harmonic vibration components D_1 and D_2 are displaced in the $-x_2$ direction, friction force F_f increases and the actuator does not move in the $-x_1$ direction even though vibration components E and F are displaced in the $-x_2$ direction.

At $\omega t = \pi/2$, when vibration components A and D_1, D_2 are displaced in the $+y_1$ and $+y_2$ directions, respectively, friction force F_f is minimal. Under these conditions, when vibration components B, C and E, F are displaced in the $+x_1$ and $+x_2$ directions, respectively, the actuator system tends to move in the $+x_1$ ($+x_2$) direction.

At $\omega t = 3\pi/2$, fundamental-wave vibration component A is displaced in the $-x_1$ direction and friction force F_f increases. On the other hand, friction force F_f decreases because second-harmonic vibration components D_1 and D_2 are displaced in the $+x_2$ direction. In addition, fundamental-wave vibration components B and C are displaced in the $-x_1$ direction and second-harmonic vibration components D_1 and D_2 are displaced in the $+x_2$ direction. The forces generated by these vibration components cancel each other and the actuator system is not expected to move. The above operation principle allows the actuator system to move in the intended direction (i.e., $+x_1$ ($+x_2$) direction) once every two cycles of the second harmonic.

The phase difference of the vibration in the state of displacement at each vibration component shown in Fig. 8 is defined as 0 degrees (in phase). Adjusting the phase difference of the vibration at vibration components A and D_1, D_2 to 180 degrees (out of phase) can reverse the direction of movement of the actuator system.

5.2 Movement Characteristics of Actuator System

The prototype actuator system was set on a surface plate and its movement characteristics were measured. Fig. 10 shows the movement speed of the actuator system in the horizontal plane when the input currents to vibration components A and D_1, D_2 were fixed at 60 and 100 mA, respectively, and the input currents to vibration components B, C, E, and F were varied. In the figure, open circles are the measurement results when the phase difference between vibration components is adjusted to be in phase (0 degrees), as shown in Fig. 8, and filled circles are the measurement results when the phase difference between vibration components is adjusted to be out of phase (180 degrees). The figure shows that the actuator system can move reciprocally at an almost constant speed.

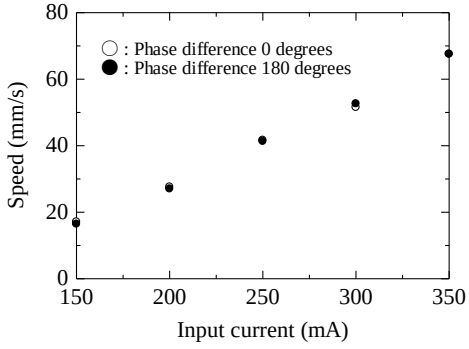

Fig. 10 Relationship between input current and speed (horizontal plane)

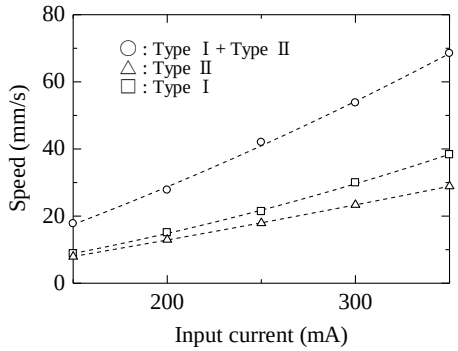

Fig. 11 Relationship between input current and speed (ceiling surface)

Fig. 11 shows the movement speed of the actuators for the ceiling surface when the input currents to vibration components A and D_1, D_2 were fixed at 60 and 100 mA, respectively, and the input currents to vibration components B, C, E, and F were varied. The phase difference between vibration components was adjusted to be in phase for the measurements. The dashed lines are the results of a quadratic approximation of the measured values obtained using the least-squares method (in following figures, dashed lines are the results of a second-order approximation obtained using the least-squares method). The square, triangle, and circle symbols are the results for type I with fundamental-wave vibration components A, B, and C driven, type II with second-harmonic vibration components D_1, D_2, E, and F driven, and a combination of types I and II, respectively. Fig. 11 shows that the movement speed increases almost linearly with increasing input current. The movement characteristics for the combination of type I and II actuators driven are considerably better than those of actuators driven only with fundamental-wave or second-harmonic vibration components.

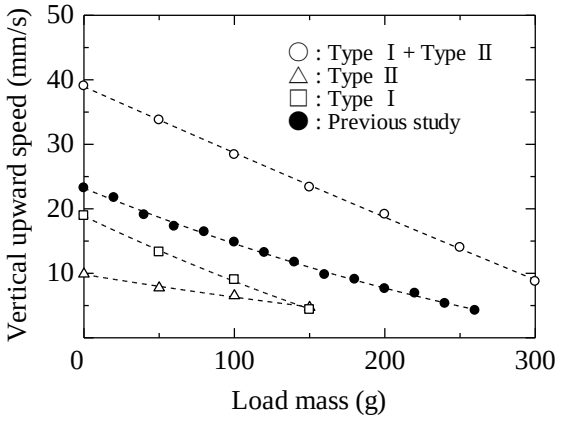

Fig. 12 Relationship between load mass and vertical upward linear speed (input current 250 mA)

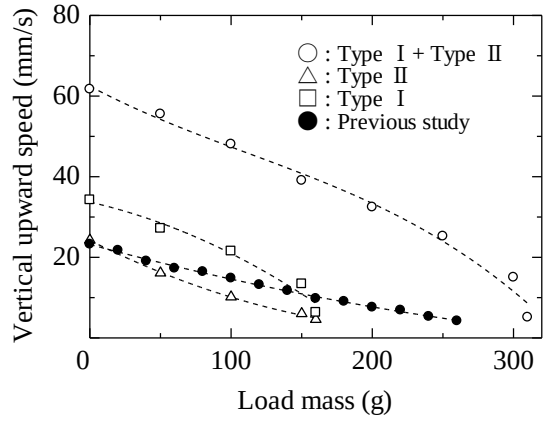

Fig. 13 Relationship between load mass and vertical upward linear speed (input current 350 mA)

Figs. 12 and 13 show the relationship between the vertical upward speed of the actuator system and the load mass when the input currents to vibration component A and vibration components D_1, D_2 were fixed at 60 and 100 mA, respectively, and the input currents to vibration components B, C, E, and Fwere fixed at 250 or 350 mA. With both type I and II actuators driven and an input current of 350 mA, the actuator system is capable of vertical upward movement at the speed of 15.1 mm/s while pulling a 300-g load mass. The solid circles in both figures are the speed values for an actuator system [15] with the same total mass of 120 g and eight fundamental-wave vibration components when an input current of 250 mA is applied to each vibration component. Due to the reduced vibration interference, the movement characteristics of the proposed actuator system greatly exceed those of the actuator system in a previous study [15].

A fundamental-wave-type actuator has a low drive frequency, which allows a large vibration amplitude with a relatively small input current. This results in the generation of large elastic energy and high movement speed. In contrast, a second-harmonic-type actuator has a high drive frequency and cannot generate a large vibration amplitude. However, it can generate a large inertial force proportional to the square of the vibration frequency. The excellent performance of the proposed actuator system is due to the effective superposition of the conflicting movement characteristics of the two types of actuator.

Based on the above, the actuator system is considered to move based on the operation principle shown in Fig. 9. This paper thus establishes a new operation principle for a phase-controlled actuator system that has good movement characteristics and can instantly switch movement direction.

6. ACTUATOR SYSTEM OPERATION PRINCIPLE AND ROTATIONAL CHARACTERTICS

The above operation principle for linear motion can be extended to rotational motion. For rotational motion in the actuator system, only the type II phase-controlled actuator was driven. As shown in Figs. 8 and 14, when vibration components D_1 and D_2 are displaced in the $+y_2$ direction, friction force F_f decreases. In this state, when vibration components E and F are displaced in the $+x_2$ and $-x_2$ directions, a moment acts on the center of the actuator system. Therefore, the system rotates counterclockwise. On the other hand, if the vibration phases of vibration components D_1 and D_2 are set to be out of phase, the system rotates clockwise.

By controlling the phase difference of the vibrations in each vibration component, the actuator system can reciprocate in all directions (i.e., 360 degrees). The rotational characteristics of the actuator system were measured by fixing the input current to vibration components D_1 and D_2 at 100 mA and varying the input current to vibration components E and F.

Fig. 15 shows the rotational speed when the actuator system was set on horizontal and vertical planes and the phase difference of the vibration between vibration components D_1, D_2 and vibration components E, F was set to 0 degrees (in phase) or 180 degrees (out of phase). In the figure, square and plus symbols (triangle and diamond symbols) are the measurement results when the phase difference between the vibration components was in phase and out of phase in the horizontal (vertical) plane, respectively. The rotational speeds of the actuator system are almost equal when the phase differences between the vibration components are in phase and out of phase. The rotational speed of the actuator system increases linearly as the input current to vibration components E and F is increased. In this actuator system, the mounting position of each vibration component is at the same distance to the center of the frame. When the actuator system is set in the vertical plane, the moments caused by gravity are canceled in each vibration component. Therefore, the rotational speeds of the actuator system in the horizontal and vertical planes are nearly equal.

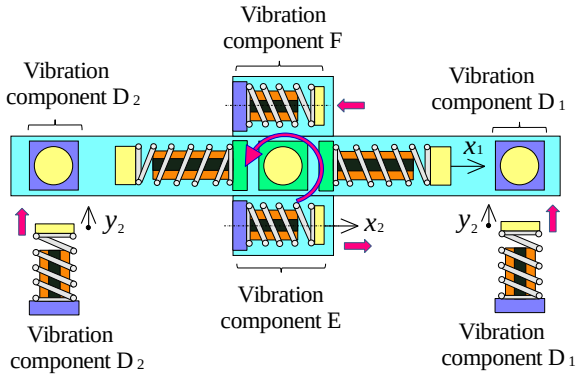

Fig. 14 Rotational principle of actuator system

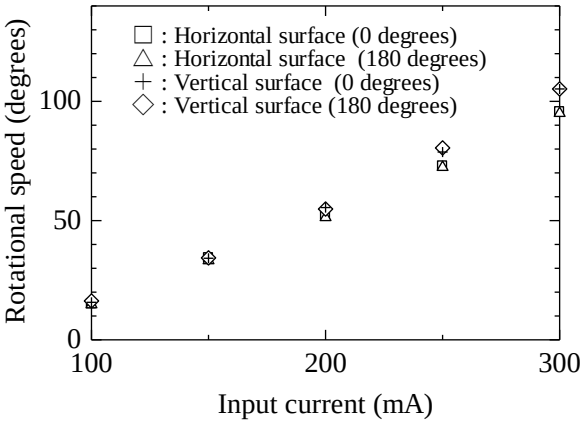

Fig. 15 Relationship between input current and rotational speed (rotational movement)

7. CONCLUSIONS

In this study, an actuator system coupled with a phase-controlled actuator with fundamental-wave and second-harmonic vibration components was proposed to improve propulsion characteristics. The operation principle of the actuator system was discussed. Based on the results of tests on prototypes, the operation principle of the phase-controlled actuator system, which can instantly switch its direction of linear motion, was established. The movement and traction characteristics of the actuator system are excellent since the vibration interference between the mounted vibration components is considerably reduced and two actuators with different characteristics are coupled.

The proposed actuator system can move vertically at a speed of 15.1 mm/s even with a load mass of 300 g. A commercially available automatic tapping device with a mass of 260 g can thus be mounted. The possibility of the internal inspection of iron structures was demonstrated through tests on prototypes. Furthermore, this actuator system can move in any direction (i.e., 360 degrees) by combining rotational and translational reciprocating motions. Because the actuator system can move on ceilings and walls, it could be useful for inspection devices.

Future work will develop a prototype phase-controlled actuator with a power-of-two-type vibration component and conduct a theoretical motion analysis that takes into account the nonlinearity of the vibration component.

8. ACKNOWLEDGMENTS

This work was supported by JSPS KAKENHI Grant Number JP23K03648.

9. REFERENCES

[1] Khirade N., Sanghi R., and Tidke D., Magnetic Wall Climbing Devices - A Review. International Conference on Advances in Engineering & Technology, 2024, pp. 55-59.

[2] Tian Y., Jitsukawa H., Ma S., and Zhang G., Magnetic Wall-Climbing Wheels With Controllable Adhesion Reduction via Soft Magnetic Material. IEEE ROBOTICS ANDAUTOMATIONLETTERS, Vol. 9, No. 12, 2024, pp. 11553-11560.

[3] Alrumayh A., Alhassoon K., and Nasser F., Electromagnetically Driven Robot for Multipurpose Applications. The Robotics Society of japan, Vol. 15, No. 2, 2025, pp. 1-15.

[4] Lin T., Chiang P., and Putranto A., Multispecies hybrid bioinspired climbing robot for wall tile inspection. Automation in Construction, 2024, Vol. 164, pp. 1-23.

[5] Yang L., Kamata S., Hoshino Y., Liu Y., and Tomioka T., Development of EV Crawler-Type Weeding Robot for Organic Onion, Agriculture, 2024, Vol. 15, No. 1, pp. 1-21.

[6] Yang P., Zhang M., Sun L., and Li X., Design and Control of a Crawler-Type Wall-Climbing Robot System for Measuring Paint Film Thickness of Offshore Wind Turbine Tower, Journal of Intelligent & Robotic Systems, 2022, Vol. 106, No. 50, pp. 316-330.

[7] Wang W., Wang K., Zhang H., and Zhang J., Internal Force Compensating Method for Wall Climbing Caterpillar Robot. in Proc., IEEE International Conference on Robotics and Automation, 2010, pp. 2816-2820.

[8] Tao C., and Liu B., Online Autonomous Motion Control of Communication-Relay UAV with Channel Prediction in Dynamic Urban Environments, Drones, 2024, Vol. 8, No. 12, pp. 1-25.

[9] Rushood M., Rahbar F., Shokri S., Selim S., and Dweiri F., Accelerating Use of Drones and Robotics in Post-Pandemic Project Supply Chain, Drones, Vol. 7, No. 55, 2023, pp. 1 - 9.

[10] Urakawa A., Sasaki T., and Cho H., Dynamic Properties of Post-Buckled Shape Memory Alloy and its Application to a Base Isolator for Vertical Vibration. International Journal of GEOMATE, Vol.20, Issue 82, 2021, pp.101-108.

[11] Furukawa A., and Goto M., Incorporatiog Poisson Effect into DEM for Enhanced numerical Analysis of Masonry of Structure. International Journal of GEOMATE, Vol. 27, Issue 119, 2024, pp. 1-9.

[12] Yaguchi H., A New Type of Electromagnetically Propelled Vibration Actuator for Appearance Inspection of Iron Structure. International Journal of GEOMATE, Vol. 20, No. 77, 2021, pp. 69 - 76.

[13] Yaguchi H., and Sato R., A New Type of Electromagnetic Vibration Actuator Capable of Combined Linear and Rotational Motion. International Journal of GEOMATE, Vol. 26, No. 117, 2024, pp. 68 - 77.

[14] Abe S., and Yaguchi H., Phased-controlled Actuator System Capable of Visual Inspection inside Iron structure, International Journal of GEOMATE, Vol. 28, No. 127, 2025, pp. 112 - 120.